Tectonophysics 497 (2011) 34–44

Contents lists available at ScienceDirect

Tectonophysics

journal homepage: www.elsevier.com/locate/tecto

U-series dating of co-seismic gypsum and submarine paleoseismology of active faults in Northern Chile (23°S)

Gabriel Vargas [a], Carlos Palacios [a,*], Martin Reich [a], Shangde Luo [b], Chuan-Chou Shen [c], Gabriel González [d], Yi-Chen Wu [b]

[a] Departamento de Geología, Facultad de Ciencias Físicas y Matemáticas, Universidad de Chile, Santiago, Chile
[b] Earth Dynamic System Research Center & Department of Earth Sciences, National Cheng-Kung University, Tainan 701, Taiwan, ROC
[c] Department of Geosciences, National Taiwan University, Taipei 106, Taiwan, ROC
[d] Departamento de Ciencias Geológicas, Facultad de Ingeniería y Ciencias Geológicas, Universidad Católica del Norte, Antofagasta, Chile

ARTICLE INFO

Article history:
Received 5 May 2009
Received in revised form 21 August 2010
Accepted 21 October 2010
Available online 31 October 2010

Keywords:
U-series dating
Submarine paleoseismology
Paleoearthquakes
Active faults
Hyperarid Atacama Desert

ABSTRACT

The convergence of the Nazca and South American plates along the subduction margin of the central Andes results in large subduction earthquakes and tectonic activity along major fault systems. Despite its relevance, the paleoseismic record of this region is scarce, hampering our understanding about the relationship between the Andes building and earthquake occurrence. In this study, we used the U-series disequilibrium method to obtain absolute ages of paleoearthquake events associated with normal displacements along the active Mejillones and Salar del Carmen faults in the Coastal Range of the Atacama Desert of northern Chile. The ^{230}Th–^{234}U disequilibrium ages in co-seismic gypsum salts sampled along the fault traces together with marine evidences indicate that earthquakes occurred at ca. 29.7 ± 1.7 ka, 11 ± 4 ka and 2.4 ± 0.8 ka. When coupled with paleoseismic marine and radiocarbon (^{14}C) records in the nearby Mejillones Bay evidencing large dislocations along the Mejillones Fault, the geochronological dataset presented here is consistent with the notion that gypsum salts formed during large earthquakes as a result of co-seismic dilatancy pumping of saline waters along the major faults. Based on maximum observed cumulative vertical offsets in the studied faults, this phenomena could have occurred episodically at a rate in the order of 1:40 to 1:50 with respect to the very large subduction earthquakes during the latest Pleistocene–Holocene period. The results presented here reveal that the U-series disequilibrium method can be successfully applied to date the gypsum salts deposited along faults during seismic events, and therefore directly constrain the age of large paleoearthquakes in hyperarid and seismically active zones.

1. Introduction

The subduction margin of the Central Andes is characterized by the occurrence of large earthquakes associated with the convergence of the Nazca and South American Plates at about 7.8 cm/year (DeMets et al., 1994; Angermann et al., 1999). This high convergence rate is responsible for causing large subduction earthquakes like the 1868 ($M_w = 8.8$) and 1877 ($M_w = 8.6$) events that affected vast areas along southern Peru and northern Chile (Dorbath et al., 1990; Comte and Pardo, 1991). In particular, the last large earthquake in 1877 ruptured ~450 km along northern Chile in a region that has been characterized ever since as a seismic gap (Kelleher, 1972; Nishenko, 1985). This rupture event stopped at the end of the Mejillones Peninsula at 23°S, which is a late Cenozoic geomorphologic feature constituted by emerged tectonic blocks limited by Quaternary faults (Armijo and Thiele, 1990; Ortlieb et al., 1996; Delouis et al., 1998; González et al., 2003). In the last decades, several large earthquakes in the hyperarid Atacama Desert of northern Chile have significantly impacted the region ($M_w = 8.1$, Antofagasta 1995 — 23°45′S/70°48′W; $M_w = 7.8$, Tarapacá 2005 — 20°05′S/69°33′W; Mw = 7.7, Tocopilla 2007 — 22°31′S/70°08′W; Fig. 1). While the 1995 subduction earthquake ruptured along 180 km southward from the Mejillones Peninsula, the 2007 Tocopilla earthquake ruptured ~150 km and ended below this feature (Ruegg et al., 1996; Delouis et al., 1997; Pritchard et al., 2006; Delouis et al., 2009), contributing moderately to the rupturing of the great northern Chile seismic gap (Delouis et al., 2009).

Because of the very recent, post-1800s population settling in the area, the historical seismic record is constrained only to a few hundred years (Comte and Pardo, 1991), limiting our knowledge about earthquake occurrence in the Atacama region of northern Chile. This is especially evident when we consider the possibility of large crustal events related to the dislocation of Quaternary faults that characterize the subduction margin. Several contributions have demonstrated spectacular geomorphologic features related to recent superficial

* Corresponding author. Tel.: +56 2 9784536.
E-mail addresses: gvargas@ing.uchile.cl (G. Vargas), cpalacio@ing.uchile.cl (C. Palacios).

0040-1951/$ – see front matter © 2010 Elsevier B.V. All rights reserved.
doi:10.1016/j.tecto.2010.10.017

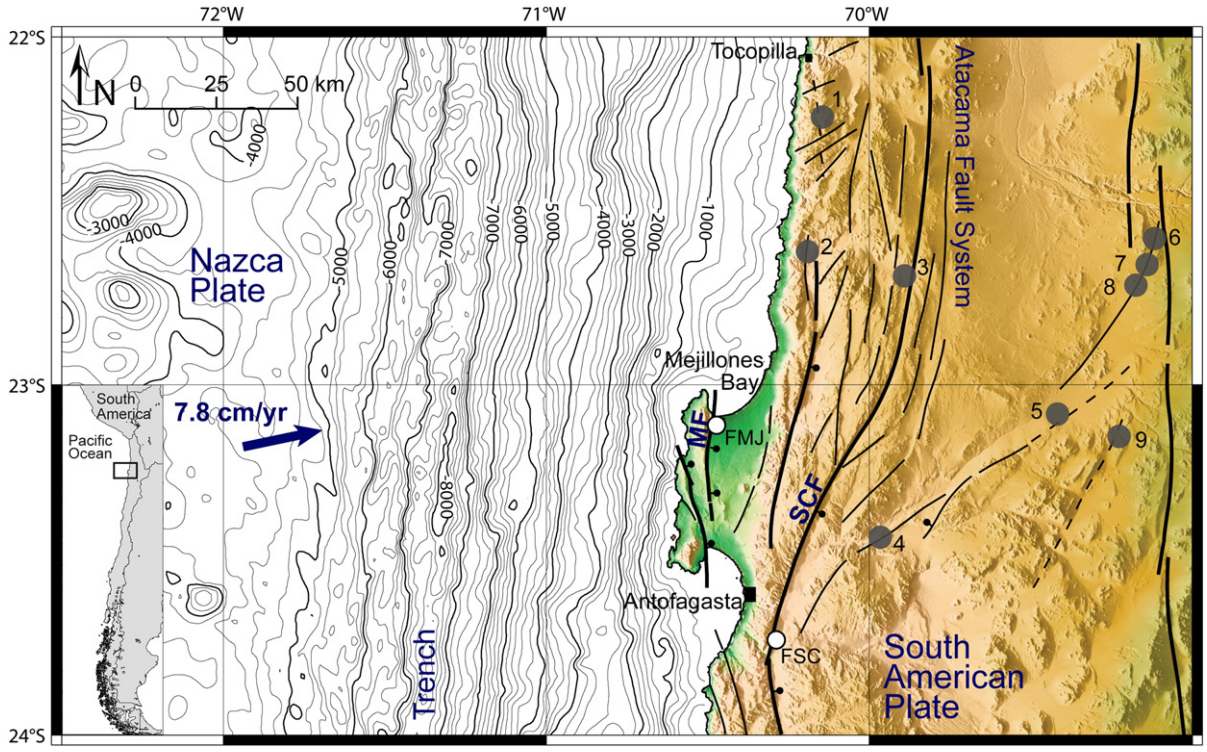

Fig. 1. Regional tectonic context of the study area, showing the Mejillones and Salar del Carmen faults (FM and SCF, respectively) and the sites of the dated co-seismic gypsum samples (FMJ-2 and 4, and FSC-1; white circles). The grey circles are Cu ore deposits referred to in the text: 1 Mantos de la Luna; 2 Michilla; 3 Antucoya; 4 Mantos Blancos; 5 Spence; 6 Radomiro Tomic; 7 Chuquicamata; 8 Mansa Mina; and 9 Gaby.
Faults from Armijo and Thiele (1990) and González et al. (2003). Tectonic plates convergence vector from DeMets et al. (1994).

tectonics and submarine fault scarps extending over several kilometers in the Coastal Range of the Atacama Desert, evidencing Quaternary faulting areas (Armijo and Thiele, 1990; Delouis et al., 1996; González et al., 2003; Marquardt et al., 2004; Allmendinger et al., 2005; Marquardt, 2005; Vargas et al., 2005; González et al., 2006). Absolute ages of single rupture events are not available (e.g. lack of vegetation prevents the use of radiocarbon techniques), limiting the determination of recurrence intervals and the short to medium-term slip rate, key elements in the evaluation of seismic hazards in the region. However, the hyperarid Atacama Desert offers an excellent opportunity to study the age of fault activity, considering the well-preserved features associated with earthquake surface flooding events.

Earthquake-induced surface flooding by groundwater in arid regions has long been recognized (Nur, 1974; Matsumoto, 1992; Muir-Wood and King, 1993; Davisson et al., 1994; Brodsky et al., 2003; Manga et al., 2003; Montgomery and Manga, 2003; Kurcer et al., 2008). Furthermore, recent studies demonstrate that saline groundwater have been forced up episodically to the surface along fault zones during earthquakes in the hyperarid Atacama Desert, depositing gypsum and halite (among other minerals) that fill fractures (Cameron et al., 2002; Palacios et al., 2005; Cameron et al., 2007; Reich et al., 2008, 2009). The extreme hyperarid conditions in the coastal Atacama Desert during the Pleistocene and Holocene (mean annual rainfall of 1–4 mm/year; Vargas et al., 2006; Reich et al., 2009), only interrupted by sporadic heavy rainfall events most commonly associated to the El Niño Southern Oscillation, ENSO (Vargas et al., 2006), suggest that pervasive gypsum dissolution is unlikely and/or negligible (MacFarlane et al., 2005; Colombani, 2008).

It is well known that faults move co-seismically at the surface during major earthquakes (e.g., Caputo and Pavlides, 2008; Chung et al., 2008; Houston et al., 2008; Taylor et al., 2008). Within this context, we studied the paleoseismic activity of the Mejillones and Salar del Carmen faults in the hyperarid core of the Atacama Desert (Fig. 1). We used the U-series disequilibrium method to constrain the timing of fissure generation related to seismic events in gypsum salts precipitated in co-seismic extensional fissures along the fault, as previously reported for late Quaternary travertine in fissures along active faults in Western Turkey (Uysal et al., 2007). We couple the U–Th data with high resolution seismic profiling data, sediment core analysis and radiocarbon dating in the nearby Mejillones Bay where the late Pleistocene–Holocene marine sediments are affected by the Mejillones Fault.

2. Tectonic and geological setting

Along the Coastal Range of northern Chile, the Atacama Fault System (AFS) is the most important structural feature and has been active since the Jurassic to the present (Arabasz, 1968, 1971; Scheuber and González, 1999). Pliocene–Quaternary tectonic extension and continental uplift have controlled the structural and morphologic evolution of the outer subduction margin of northern Chile, including the activity of major faults such as the Mejillones and Salar del Carmen faults in the Coastal Range (Armijo and Thiele, 1990; Delouis et al., 1996; Ortlieb et al., 1996; González et al., 2003, 2006). These two faults form a suite of normal structures which exert a strong control on the morphology of the outer forearc of this part of the Central Andes. Cumulative vertical displacements along these faults produce ca. 300–400 m height Miocene–Pleistocene mountain fronts along the Coastal Range and Mejillones Peninsula. The Salar del Carmen Fault (SCF) constitutes one of the main strands of the AFS (Figs. 1 and 2). It strikes between N5°W and N20°E, and dips 75°E, reaching at least 40 km along strike (Fig. 1). The SCF displaces inactive alluvial fans which form part of the eastern piedmont of the Coastal Range (Fig. 2). Along this structure an east facing fault scarp with a maximum height of 9 m is attained (González et al., 2003, 2006). The Mejillones Fault (MF) is sub-parallel to the SCF bordering to the west the Mejillones plain, which is characterized by uplifted Quaternary litoral sediments, topographically depressed with respect to the marine terraces in the mountain ridge located immediately to the west of the MF (Armijo

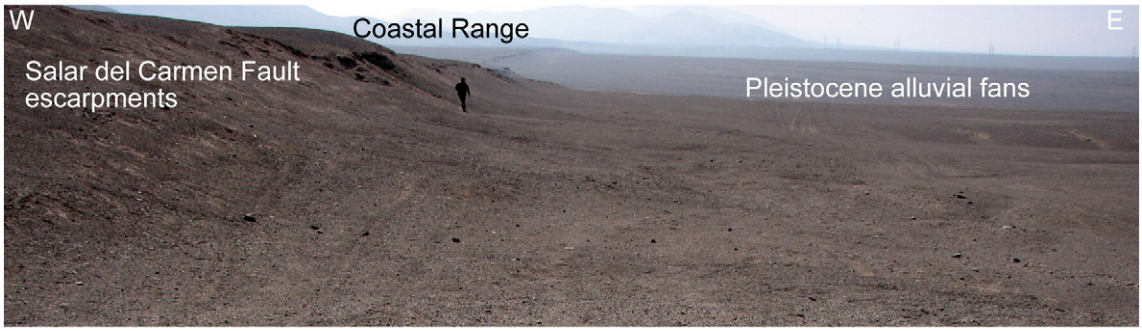

Fig. 2. Photograph showing fault escarpments along the Salar del Carmen Fault, located at the eastern limit of the Coastal Range, which affect Pleistocene alluvial fans.

and Thiele, 1990; Ortlieb et al., 1996; Figs. 1 and 3). Recent activity along the MF is also expressed in the topography by 15 km long segment, which exhibits conspicuous composed fault scarps with a cumulative vertical displacement varying between 2 and 19 m cutting Quaternary alluvial units (Armijo and Thiele, 1990; Ortlieb et al., 1996; Delouis et al., 1998; González et al., 2003; Marquardt, 2005; Fig. 3). Both major faults exhibit dip-slip striae and their most recent slip is represented by east-side down vertical displacement of Quaternary alluvial surfaces.

Although several studies regarding the local Neogene tectonics of the Mejillones Peninsula and the nearby Coastal Range have been published (e.g. Armijo and Thiele, 1990; González et al., 2003; Marquardt, 2005; González et al., 2006), systematic investigations of paleoseismic events along these faults are based on indirect dating such as: i) The minimum age of two displaced fan surfaces along the MF (26.3 ± 1.7 ka and 46.5 ± 1.7 ka; ^{10}Be in quartz dating; Marquardt, 2005), ii) seismic reflection profile data from Mejillones Bay, from which Vargas et al. (2005) inferred a large earthquake occurring shortly after the middle Holocene associated with the MF, and iii) the maximum age of faulting along the SCF, using ^{21}Ne in quartz dating from displaced alluvial surfaces (400 ka; González et al., 2006).

3. Gypsum salt filling of fault zones in the Atacama Desert and evidence for seismic pumping

Earthquakes have been observed to affect hydrological systems in a variety of ways. Changes in water levels, discharge rates or temperature have been reported following tectonic earthquakes, and recent studies have reported that permeability at the site can increase by a factor of three at the time of the earthquake (e.g. Wakita, 1975; Mogi et al., 1989; Muir-Wood, 1994; Roeloffs, 1998; Elkhoury et al., 2006; Ohno et al., 2006). Surface flooding by groundwater during seismic events has long been recognized (Sibson et al., 1975; Sibson, 1981), and various studies have documented the episodic uprise of highly saline water along fault zones and co-seismic precipitation of salt deposits (Uysal et al., 2007; Kurcer et al., 2008). In addition, effects of faulting on geothermal waters including stress modeling, effects of the internal structure of fault zones on permeability and potential fluid transport have been recently investigated by Gudmundsson et al. (2009).

In the Atacama Desert, salt minerals that fill fractures along active faults can be followed for hundred of meters (and even kilometers) along the fault trace and associated minor fractures. Near-vertical fractures within the major faults are filled with gypsarenite, gypsum and/or halite, exhibiting lamination parallel to the walls of the fractures and gypsum crystals growing perpendicular to the fracture boundaries. The salts precipitated in fault zones and fractures have been interpreted as the result of ascending saline groundwater triggered by seismic pumping during large earthquakes (Cameron et al., 2002; Palacios et al., 2005; Cameron et al., 2007; Reich et al., 2008, 2009). A more extensive surface saline cover in the Atacama Desert has been documented as deflated gypsum rich soil from the saline fog in the coastal area (Rech et al., 2006).

Additional observations in Cu ore deposits indicate that the salt-filled fractures extend vertically over 300 m of supergene enrichment caps, in which commonly the veins maintain their thickness (Reich et al., 2009). The upward flow that deposited gypsum along fault zones is supported by the following geochemical and mineralogical evidence from ore deposits in the Antofagasta region (Fig. 1): i) Strong geochemical soil-rich surface anomalies along the faults that traverse the Mansa Mina, Radomiro Tomic, Gaby, Spence and Mantos Blancos copper deposits, involving Cu, Mo, S, Re, Na, Cl, Se, I, and Br, that are restricted to a few meters across the active fault (Cameron et al., 2002; Palacios et al., 2005), ii) fluid inclusions on atacamite intergrown with gypsum from veins within faults in the leached zone of the Mantos Blancos and Spence copper porphyries, indicating salinities that strongly

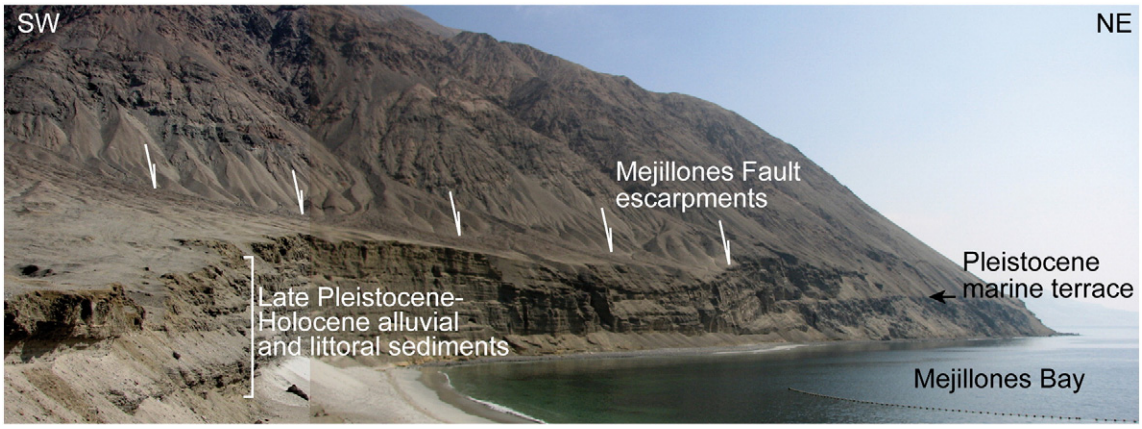

Fig. 3. Photograph showing a general view of fault escarpments along the Mejillones Fault, cut littoral and alluvial fans, and the Mejillones Bay.

correlate with the salinities at which gypsum supersaturates from groundwater in both deposits (Reich et al., 2008), iii) ^{36}Cl isotopic data on gypsum–atacamite assemblages from various copper ore deposits showing low ^{36}Cl-to-Cl ratios, comparable to previously reported values of deep old groundwaters (Reich et al., 2008), iv) present-day geochemical and isotopic data of groundwaters at the Spence deposit supporting a deep origin for the water involved in supergene oxidation of the pre-existing copper ores (Leybourne and Cameron, 2006, 2008; Reich et al., 2008, 2009), and v) the ^{230} Th–^{234} U ages of gypsum intergrown with atacamite in supergene veins from copper deposits cluster at 240 ka for the Chuquicamata, 130 ka for the Mantos Blancos and Spence, and 80 ka for Mantos de la Luna and Michilla copper orebodies, indicating that supergene Cu enrichment also occurred during hyperarid climatic conditions, when groundwater passed up through and modified the pre-existing supergene Cu oxide minerals (Reich et al., 2009).

4. Sampling and U–Th series dating

In the Mejillones and Salar del Carmen faults (MF and SCF, respectively) we collected material directly from the main fault plane outcrops. In the MF two samples were collected (FMJ-2 and FMJ-4) from gypsum veins that fill the main fault plane, which is exposed in a trench excavated in correspondence with a 3–5 m fault scarp (Fig. 4). In the case of the MF, bands of gypsum and halite are disposed in centimetric veins parallel to fault planes with striae indicating normal slip mechanism, with gypsum showing cleavage perpendicular to the fractures. Halite crystals are intergrowth in between the gypsum bands and also form breccias with fragments of metamorphic rocks, which are disposed along the main fault plane on N15°E/57°E. The FSC-1 sample was obtained from a gypsum vein that fills the main fault plane of the SCF which is N31°E/77°E exposed in the wall of an alluvial channel, where a vertical offset of 3 m and a fault scarp of at least 1 m in height can be observed. In this case centimetric gypsum veins are parallel to the main fault plane, and massive halite is localized in between involving centimetric fragments of alluvial sediments. These veins are connected with superficial efflorescences which are observed for several kilometres along the main fault trace (Fig. 5). The difference between the total offset and height of the scarp could be attributed to partial erosion of the fault scarp during slip progression (Fig. 5). Detailed mineralogical observations of the gypsum breccias sampled at Mantos Blancos, located on the Antofagasta–Calama Lineament, near the SCF (Figs. 1 and 6A), show that gypsum is intimately intergrown with atacamite at the micron to nano-scales (Fig. 6B–D), with no evidence of dissolution and/or reprecipitation.

Gypsum samples were dated using the U–Th series disequilibrium method (Ku, 1976; Luo and Ku, 1991; Ku et al., 1998). The method has been successfully applied to obtain absolute ages of formation of salt minerals that precipitate from aqueous solutions (e.g. gypsum and halite), in a range that falls between <10 and 350 kyrs (Ku et al., 1998). The U–Th series method requires simultaneous measurements of the degree of radioactive disequilibrium between ^{230}Th and ^{234}U and between ^{234}U and ^{238}U in the salt minerals. However, age uncertainties can arise due to the presence of inclusions or clays in the samples containing detrital ^{230}Th and ^{234}U, and the required closed system condition for the isotopes of interest is not ensured due to recrystallization or dissolution of the minerals. These potential difficulties were overcome by analyzing only primary gypsum in veins and veinlets, with no evidence of recrystallization or dissolution.

Gypsum crystals were hand-picked, separated, and inspected using a petrographic microscope and X-ray diffraction techniques. The methods used for U-series dating of gypsum followed the isochron approach of Luo and Ku (1991) that corrects for initial ^{230}Th contamination.The

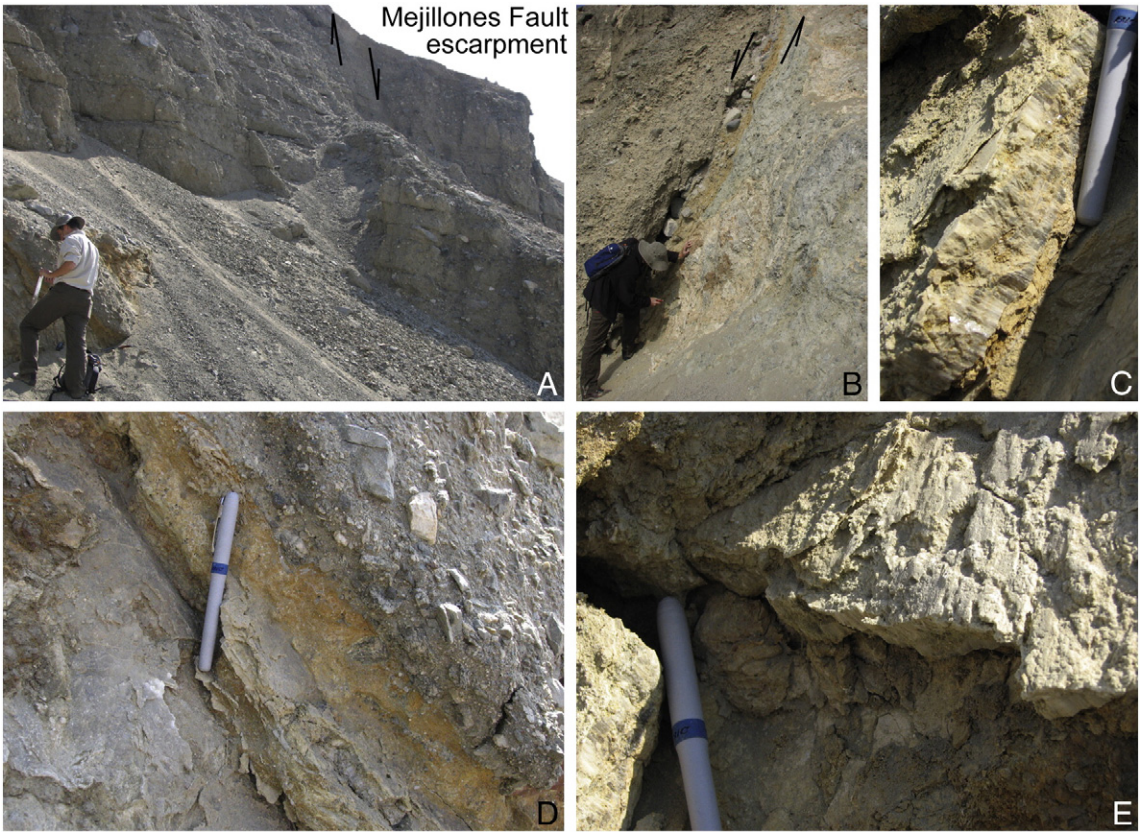

Fig. 4. (A, B) View of outcrops of samples sites along the Mejillones Fault (MF). (C, D) Details of gypsum vein along the MF, and internal structure of salt, showing gypsum crystals growing perpendicular to the fracture boundaries. (E) Striae in fault planes with gypsum.

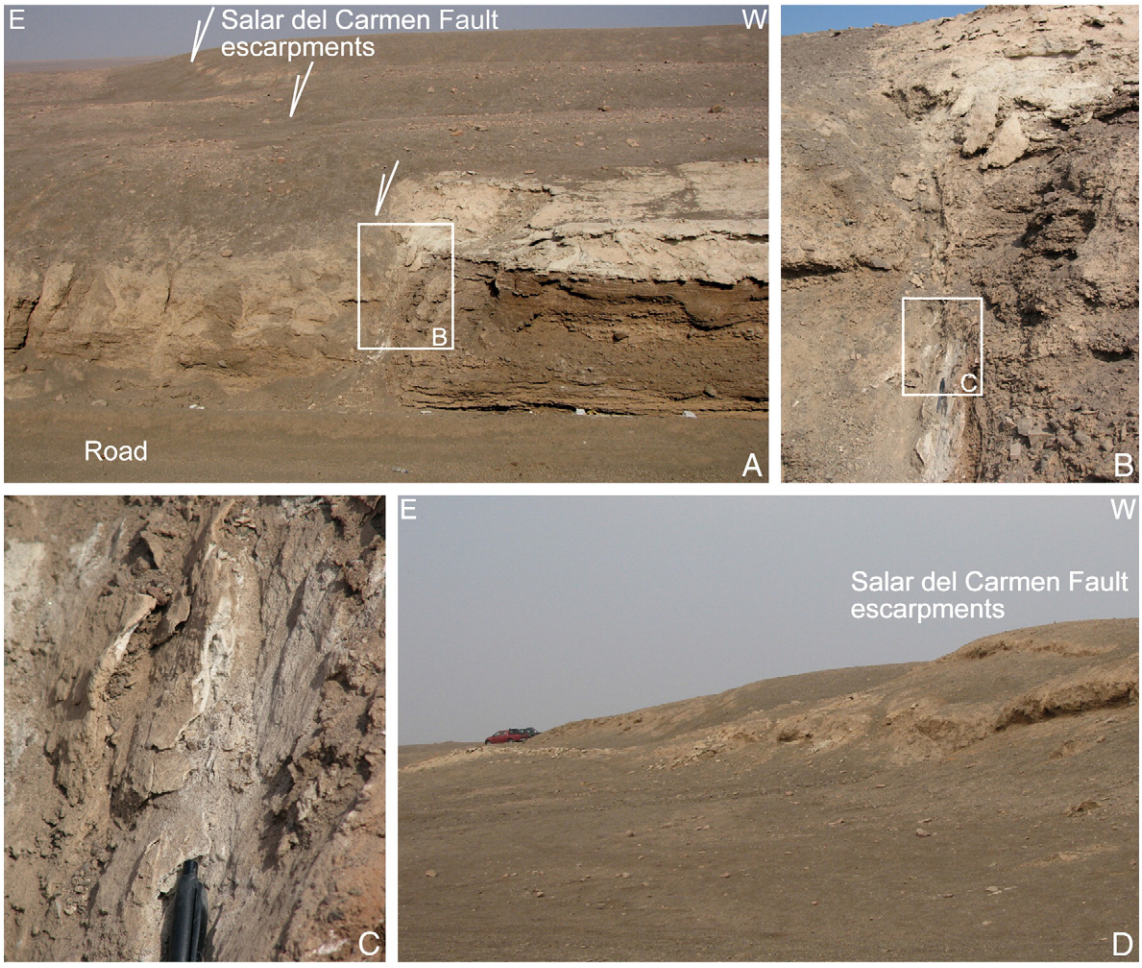

Fig. 5. (A, B, C) Salt ridge along fault escarpments of the SCF, showing efflorescence and gypsum veins sampled for U–Th analyses. (D) Additional view of fault escarpments with efflorescence located along strike.

analytical work was performed using a Multi-collector Inductively Coupled Plasma Mass Spectrometer MC-ICP-MS (Thermo Neptune) at the High-precision Mass Spectrometry and Environment Change Laboratory (HISPEC), National Taiwan University. The chemical methods followed the approach of Luo and Ku (1991), Cheng et al. (2000) and Shen et al. (2002, 2003). Measurements of U and Th isotopes are shown in Table 1.

5. Results and discussion

5.1. U–Th series ages and seismic pumping

Three gypsum samples from veins in fault outcrops of the MF and SCF were dated, and the location of the samples is shown in Fig. 1. The estimated isochron ages are presented in Table 2, and show that the gypsum salts collected in the MF and SCF were formed in the last 50 thousand years. The samples from the MF (FMJ-2 and FMJ-4) indicate isochron ages of 3.1 ± 0.8 ka and 29.7 ± 1.7 ka, respectively. The gypsum samples FSC-1 from the SCF gave an age <2.5 ka.

Recent $\delta^{34}S$ data on gypsum from veins and co-seismic crack fill material evidence values between 3.7 and 9.4‰, which are similar to groundwater, and different to the common salt soil in the Atacama Desert (Rech et al., 2009). These isotopic data suggest that gypsum that precipitated in fractures zones and cracks derived from groundwater pumped to the surface during seismic events. Seismic or "cyclical dilatancy" pumping involves strain cycling to explain effusions of water after earthquakes (Sibson, 1981). Tectonic extension produces fractures in the brittle upper crust that provide pathways for groundwater migration and storage. During earthquakes, local stress fields become compressional, closing fractures and forcing groundwater along faults and fractures to areas of lower pressure, typically towards the surface. Given the low permeability of basement rocks, groundwater migrates slowly to faults, resulting in continued effusion for weeks following an earthquake. This increased flow occurs in regions where the pre-seismic water table lies at moderate depth (e.g. <50 m), under semi-arid to wetter climate conditions.

Observations at the Salar del Carmen Fault (Fig. 6) in the Mantos Blancos deposit provide striking examples of advective transport along faults in hyperarid areas. At Mantos Blancos, the water table lies at 400 m depth; therefore, injection of water into the base of narrow, air-filled fractures that extend 400 m to the surface could cause mixing of air with the saline waters producing turbulent flow of the mixture, as suggested by Cameron et al. (2010). This tectonically-driven surges of compressible, brine/air mixture speed up during ascent from a variable base level of 500–50 m (the current depth of groundwater tables in the Atacama Desert), until pressure drop near the surface produces supersaturation and precipitation of gypsum in short timescales (<1 year).

5.2. Paleoseismological implications

When coupled with additional data and field observations, the U–Th dating of gypsum along the MF (FMJ-2 and FMJ-4) suggests co-seismic fault dislocations during the late Pleistocene–Holocene period, at 29.7 ± 1.7 ka and at 3.1 ± 0.8 ka. Alluvial fans located in the piedmont of the mountains at the eastern flank of the Mejillones Peninsula, which are cut

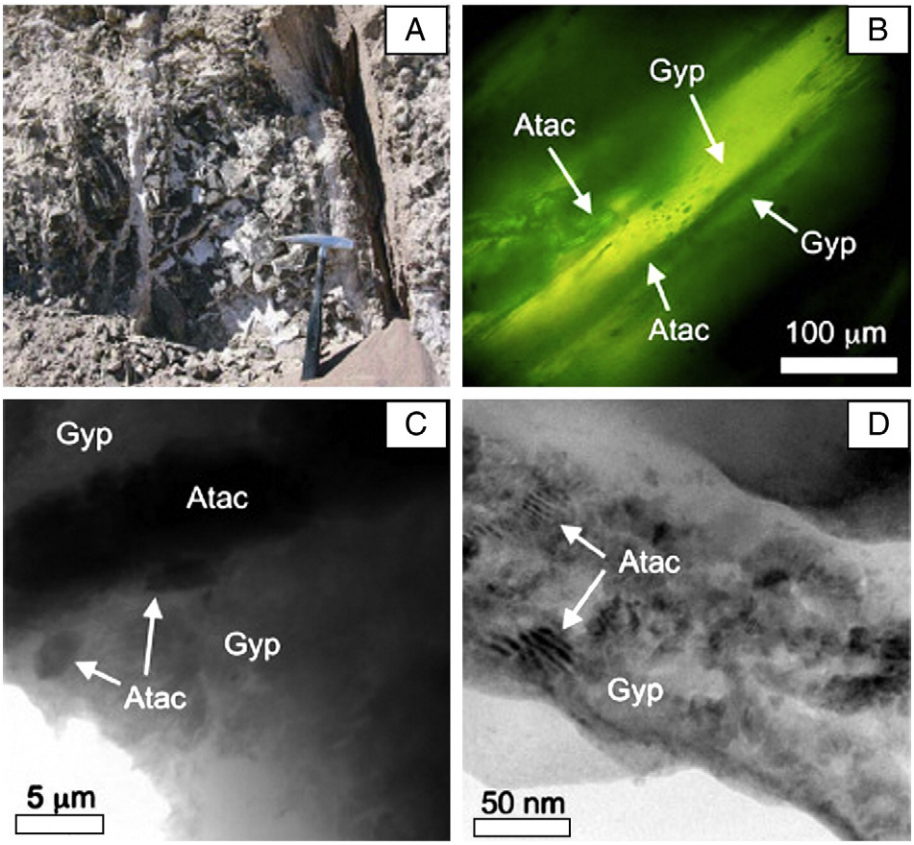

Fig. 6. (A) Gypsum-atacamite breccias from the Mantos Blancos Cu deposit, located on the Antofagasta–Calama Lineament, near the Salar del Carmen Fault (see Fig. 1). (B) Reflected-light polarizing microscopy image showing gypsum (Gyp)-atacamite (Atac) bands at microscale. (C, D) Bright-field transmission electron microscopy (TEM) images showing the gypsum–atacamite banding at the nanoscale. The composition of gypsum and atacamite was confirmed by energy-dispersive spectrometry (EDS). The TEM data were collected using a Tecnai F20 FEG-TEM at the Department of Geology, University of Chile. The TEM was operated at 200 kV, with an EDAX EDS (EDS ~1 wt.% detection limit). Chlorine-36 and U-series disequilibrium isotopic data reported by Reich et al. (2008, 2009) indicate that gypsum/atacamite assemblages at Mantos Blancos were deposited by saline, deep formation waters.

by the MF, indicate that this structure has been active during the Late Pleistocene (Armijo and Thiele, 1990; Marquardt, 2005). Recent field observations revealed at least three alluvial surfaces affected by faults along the main trace of the MF (Fig. 7). While no ages are available for the most recent alluvial unit, ^{10}Be exposure dates in the two cut fan surfaces near the sampled sites provided mean values of 46.5 ± 3.7 ka and 26.3 ± 1.7 ka (Marquardt, 2005). The apparent chronostratigraphic agreement between the absolute and relative ages of the three alluvial surfaces affected by the MF and the U–Th ages of co-seismic gypsum in the same fault system, suggests that this data represent the latest rupture events along this structure, which occurred during the late Pleistocene–Holocene period.

Ongoing studies from submarine fault scarps and deformed marine sediments in the Mejillones Bay provide additional support for a Late Holocene and also a probably a latest Pleistocene rupture along the MF (Fig. 8). Taking into account the mass accumulation rates estimated from the analysis of short cores in sediments from this marine basin and considering the late Quaternary age of the whole upper seismic unit, it is clear that a seismic event occurred shortly after the middle Holocene, as revealed through high resolution 12 kHz sub-bottom profile data (Vargas et al., 2005).

New radiocarbon (^{14}C) data in a 6 m long sediment core recently obtained in the bay gave conventional ages of 2350 ± 40 and 2290 ± 30 (OS-62858 and OS-62857, respectively, NOSAMS, National Ocean

Table 1
Measurements of U and Th concentrations and activity ratios in gypsum samples by MC-ICP-MS.

Sample no.	Subsample no.	^{238}U (ppb)	^{232}Th (ppb)	(^{234}U/^{238}U)	(^{230}Th/^{234}U)	(^{230}Th/^{232}Th)	(^{234}U/^{232}Th)	(^{238}U/^{232}Th)
FSC-1 (gypsum)	SC1-1	2363 ± 8	3336 ± 10	0.993 ± 0.002	0.574 ± 0.003	1.234 ± 0.006	2.149 ± 0.008	2.164 ± 0.009
	SC1-2	628 ± 2	907 ± 3	0.993 ± 0.002	0.617 ± 0.003	1.296 ± 0.006	2.106 ± 0.007	2.121 ± 0.010
	SC1-3	1315 ± 5	2808 ± 7	0.987 ± 0.002	0.909 ± 0.005	1.285 ± 0.005	1.415 ± 0.005	1.434 ± 0.006
	SC1-4	1377 ± 3	3005 ± 9	0.988 ± 0.002	0.924 ± 0.005	1.278 ± 0.006	1.385 ± 0.005	1.402 ± 0.005
FMJ-2 (gypsum)	MJ2-1	32.40 ± 0.06	13.1 ± 0.01	1.085 ± 0.003	0.254 ± 0.001	2.078 ± 0.007	8.424 ± 0.022	7.766 ± 0.016
	MJ2-2	19.64 ± 0.03	14.6 ± 0.01	1.068 ± 0.002	0.475 ± 0.002	2.093 ± 0.008	4.632 ± 0.010	4.339 ± 0.008
	MJ2-3	14.20 ± 0.03	29.9 ± 0.02	1.076 ± 0.002	1.142 ± 0.006	1.786 ± 0.007	1.762 ± 0.004	1.637 ± 0.003
	MJ2-4	76.11 ± 0.15	102.0 ± 0.08	1.021 ± 0.002	0.891 ± 0.004	2.074 ± 0.008	2.390 ± 0.006	2.341 ± 0.005
FMJ-4 (gypsum)	MJ4-1	20.51 ± 0.04	15.55 ± 0.01	1.057 ± 0.002	0.653 ± 0.003	2.781 ± 0.008	4.477 ± 0.010	4.236 ± 0.009
	MJ4-1*	20.51 ± 0.04	15.65 ± 0.04	1.057 ± 0.002	0.653 ± 0.003	2.763 ± 0.014	4.449 ± 0.014	4.209 ± 0.013
	MJ4-2	35.12 ± 0.06	31.25 ± 0.03	1.059 ± 0.002	0.700 ± 0.003	2.544 ± 0.008	3.744 ± 0.008	3.537 ± 0.007
	MJ4-3	61.69 ± 0.12	77.31 ± 0.07	1.038 ± 0.002	0.925 ± 0.004	2.343 ± 0.008	2.610 ± 0.006	2.514 ± 0.005
	MJ4-4	106.5 ± 0.2	134.0 ± 1.1	1.039 ± 0.002	0.888 ± 0.029	2.242 ± 0.076	2.569 ± 0.022	2.472 ± 0.021
	MJ4-4*	106.5 ± 0.2	132.2 ± 0.2	1.039 ± 0.002	0.926 ± 0.004	2.369 ± 0.010	2.605 ± 0.006	2.507 ± 0.006

Table 2
Non-detrital activity ratios of $^{230}Th/^{234}U$ and $^{234}U/^{238}U$ derived from the slopes of isochron plots and the estimated ages of the gypsum.

Sample no.	($^{234}U/^{238}U$)	($^{230}Th/^{234}U$)	Age (ka)
FSC-1	1.0035 ± 0.0010	-0.024 ± 0.023	<2.5
FMJ-2	1.0961 ± 0.0012	0.028 ± 0.007	3.1 ± 0.8
FMJ-4	1.0848 ± 0.0008	0.240 ± 0.012	29.7 ± 1.7

Sciences Accelerator Mass Spectrometer Facility at Woods Hole Oceanographic Institution), from layers located just on top of the upper large slump associated with deformed stratigraphic horizons affected by the MF (Fig. 8). The calibrated ages gave values of 1600 ± 90 cal. BP and 1670 ± 120 cal. BP, from layers located at 317 and 319 cm of core depth respectively, taken a ΔR of 262 ± 13 years (Vargas et al., 2007), and using the Calib 6.0.1 program (Stuiver and Reimer, 1993). These values are close to the young U–Th age of 3.1 ± 0.8 ka obtained from co-seismic gypsum, and supports the idea that a late Holocene earthquake along the MF deformed the most recent strata of the Holocene sedimentary infill in the Mejillones Bay and induced gravity instability and slumping within the bay bottom (Vargas et al., 2005). Considering the U–Th age and the calibrated radiocarbon data, we dated the last event in the MF as 2.4 ± 0.8 ka, but it probably occurred close to the calibrated radiocarbon age of 1.67 ± 0.12 cal. ka BP, if we consider that dated layers in core GC3 directly overlay deformed sediments associated to submarine fault scarps (Fig. 8).

Additionally, the sub-bottom profile data showed a large slump deposit associated with deformed stratigraphic horizons at the foot of a composed submarine fault scarp along the trace of the MF (Fig. 8). The seismic stratigraphy of the inner part of the bay is characterized by an angular unconformity probably associated to erosion during at least the last late Pleistocene low sea level stand, when the global sea level was located ca. −120 m with respect to the present (20–18 ka, Lambeck et al., 2002; Fig. 8). The upper late Quaternary sedimentary infill overlying Neogene sediments that can be observed in the sub-bottom profiles (Fig. 8), can be divided in two units: The Lower, which develops onlap termination of strata and exhibits an aggradational depositional architecture, towards the margin of the marine basin, and the Upper, which is characterized by downlap terminations and proggradates toward the inner part of the basin (Fig. 8). Thus, considering the available radiocarbon ages together with the depositional characteristics of both units, it is probable that most of the Lower Unit in the sedimentary infill of this basin was formed concomitantly with a rising sea level during the period coeval to the global deglaciation, between 15 and 7 ka, while the Upper Unit represents the proggradation of the marine sedimentary system during the Holocene high sea level stand after 7 ka (Lambeck et al., 2002). Considering this hypothesis, the large slump deposit associated with deformed stratigraphic horizons located at the base of Lower Unit may represents a rupture event occurred at 11 ± 4 ka along the MF.

Alluvial surfaces cut by the MF close to the Mejillones Bay exhibit composed fault scarps with maximum accumulated vertical offset of 19 and 13 m with respect to the modern depositional unit (Fig. 7), and submarine fault scarps exhibit maximum vertical offset of ca. 13.7 m, as observed in sub-bottom profiles from the Mejillones Bay (Fig. 8). Considering the exposure ^{10}Be-age of 46 and 26 ka for the two conspicuous cut alluvial surfaces (Marquardt, 2005), and taking into account maximum observed cumulative vertical offsets for those surfaces, a maximum preliminary mean slip rate in the order of 0.4–0.5 m/ka can be estimated along this normal fault since the Late Pleistocene. If we consider three large events in the last 29 ka, probably four during the last 46 ka, and taking into account maximum lengths in the order of 15 km for the fault segments of the MF (Armijo and Thiele,

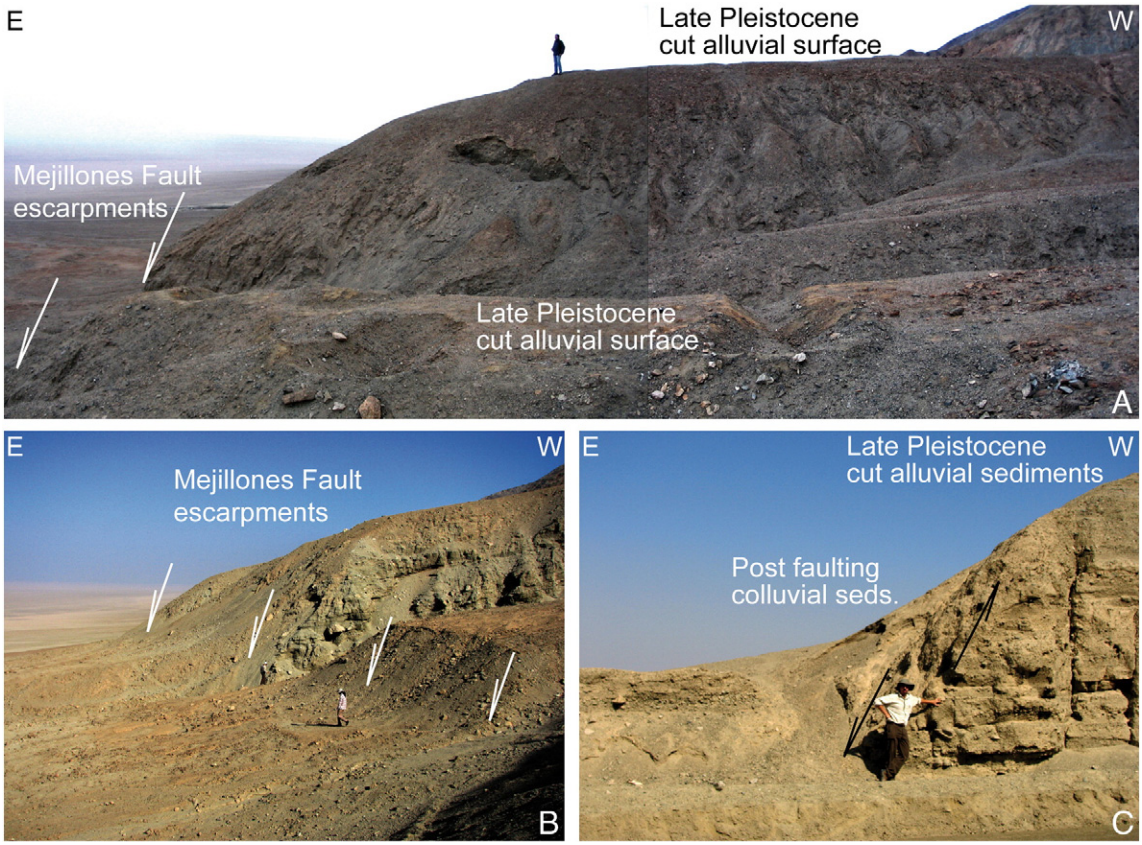

Fig. 7. Photographs showing cut alluvial fans with associated Mejillones Fault escarpments. (A, B) Views showing cut alluvial surfaces of Late Pleistocene inferred age (Marquardt, 2005). (C) Detail of alluvial sediments and a recent fault escarpment.

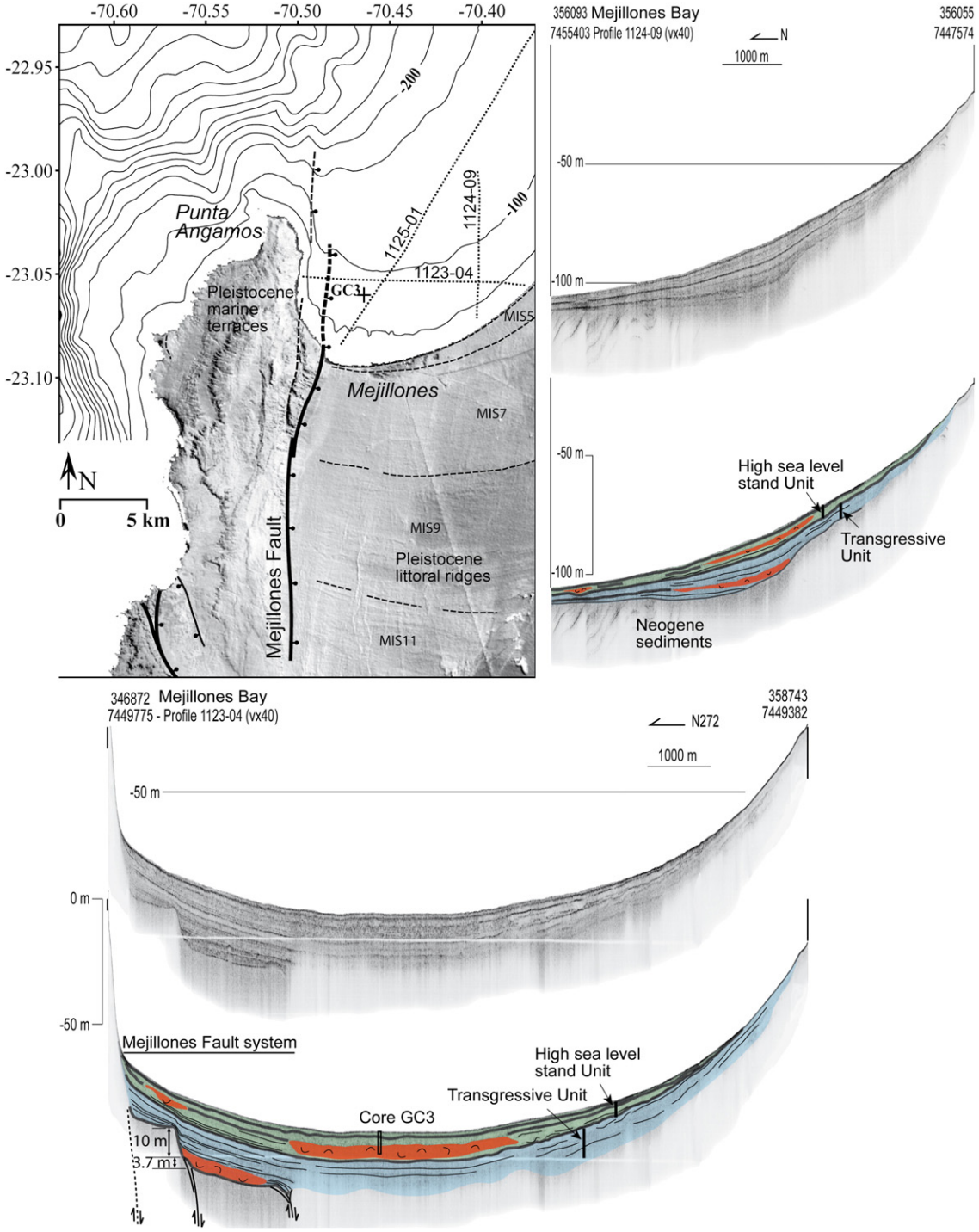

Fig. 8. Sub-bottom profiles from the Mejillones Bay realized using a 12 kHz Bathy2000 device and location of a 6 m long sediment core (GC3) obtained from this basin. Conventional radiocarbon ages in this sediment core from layers located just on top of the upper large slump deposit, gave values of 2350 ± 40 and 2290 ± 30 BP. Profile 1125-01 is shown in Vargas et al. (2005).
Distribution of littoral ridges assigned to MIS5-11 according Ortlieb et al. (1996). Mejillones Fault traces according Armijo and Thiele (1990), González et al. (2003) and Vargas et al. (2005).

1990; González et al., 2003; Fig. 1), the maximum expected magnitudes for each of this earthquake events could be in the order of M = 6–7, with associated metric scale displacements according scale relationships between earthquakes and fault geometry (Wells and Coppersmith, 1994). Although these estimations must be revised taking into account a more detailed mapping of fault segments and their corresponding kinematics, such a magnitude associated with superficial ruptures along the MF can explain the occurrence of large, meters-thick submarine slump deposits, with respect to the much smaller scale centimeters to decimeters-thick sedimentary records associated to large subduction earthquakes (Vargas et al., 2005). Thus, the displacement history of the Mejillones Fault during the late Pleistocene–Holocene period, deduced from the quantification and comparison of submarine fault scarps and cut alluvial surfaces (Figs. 7 and 8), can be explained by large earthquakes (M_w6–7) with recurrence intervals at several thousand years scale (Fig. 9).

The gypsum sample FSC-1 from the Salar del Carmen Fault indicates an age < 2.5 ka, suggesting an earthquake event during the late Holocene

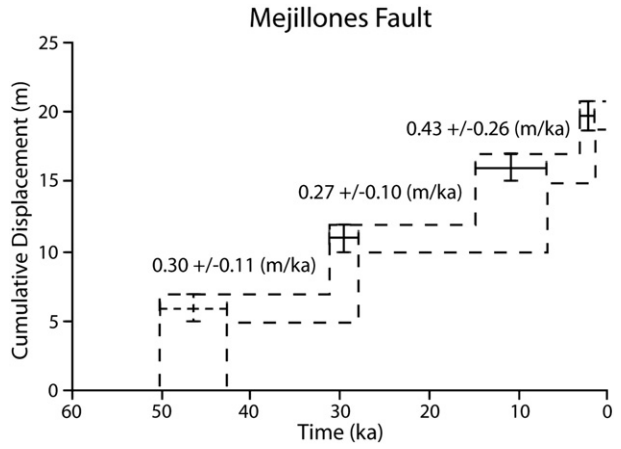

Fig. 9. Cumulative displacement history of the Mejillones Fault associated to large earthquakes in this structure during the late Pleistocene and Holocene period, as suggested from the quantification of submarine fault scarps and cut alluvial surfaces. Ages inferred from U–Th series and marine radiocarbon data (29.7 ± 1.7 ka and 2.4 ± 0.8 ka), together with 12 kHz sub-bottom profile data (11 ± 4 ka). A maximum ^{10}Be exposure age from cut alluvial surface is also considered (Marquardt, 2005; ca. 46 ka, doted point).

along this fault. In the SCF zone, recent activity was responsible for the construction of piedmonts, as evidenced by older inactive alluvial fans cross-cut by younger alluvial fans that have their apices localized along the main scarp. In turn, colluvial wedges derived from the degradation of the main scarp are affected by normal faults (González et al., 2006), suggesting recent superficial rupture along this fault. Our data also indicate a roughly contemporary paleoseismic event along the MF and SCF, suggesting coeval dislocations of both major structures during the late Holocene.

Superficial manifestations of cracks and fractures with centimeter to decimeter scale displacements observed along some of the major faults in the Atacama Fault System, have been associated to medium-large subduction earthquakes, as for the last Antofagasta and Tocopilla earthquakes, occurred on 1995 and 2007, respectively (Delouis et al., 1998; Loveless et al., 2009). In spite of that, no evidence of flooding or efflorescence formation has been reported along the surface trace of the faults. This lack of evidence for surface manifestation of significant tectonic pumping along major faults during large subduction earthquakes, in particular during the 1995 Antofagasta seismic episode, provides additional support to the idea that hydrofracture and hydraulic pumping of groundwater occurs when major faults becomes seismically active during localized large earthquakes, depositing gypsum and halite in veins and breccias along the fault planes, contributing to efflorescence and crust soil formation on surface. Thus, the available data suggests three large seismic events in the last 29 ka, eventually four in the last 46 ka, which can be interpreted as earthquakes induced by fault dislocations along the MF. Although reliable historic seismic data about the occurrence of large subduction earthquakes in northern Chile is almost lacking, or reduced to a couple of centuries (Comte and Pardo, 1991), recent paleoseismological record from previous and ongoing research from marine sediment cores off the Central Andes, including the Mejillones Bay (23°S), suggests that the timing for the occurrence of very large subduction earthquakes could be in the order of 250–300 years (Vargas et al., 2005). This implies that the ratio for the occurrence of large earthquakes along major faults, as in the MF, with respect to large subduction earthquakes, like the 1877 event, could be in the order of 1:40 to 1:50. Even if large seismic events along major faults are triggered by extension during large subduction earthquakes or during the relaxation or the interseismic period (Delouis et al., 1998; Chlieh et al., 2004; Pritchard et al., 2006; Loveless and Pritchard, 2008), our data shows that the activity of those faults account for a part of the inelastic lithospheric deformation in the subduction margin, which results in spectacular geomorphologic features, as the differentiated uplifted littoral ridges and marine terraces in the Mejillones Peninsula (Armijo and Thiele, 1990; Ortlieb et al., 1996), at long term — Quaternary — time scale.

6. Conclusions

Based on U-series disequilibirum dating of co-seismic gypsum filling fractures and fault plains, together with high resolution seismic profile data and calibrated marine radiocarbon ages, from layers directly overlaying deformed sediments associated with submarine fault scarps, we conclude that large paleoearthquakes occurred at ca. 29.7 ± 1.7 ka, at 11 ± 4 ka and at 2.4 ± 0.8 ka (3.1 ± 0.8–1.67 ± 0.12 ka) along the Mejillones Fault. In particular, a close match between the marine radiocarbon data and the U–Th isochron ages is observed along this fault system for the latest large earthquake episode during the late Holocene, and also suggests a recent roughly coetaneous dislocation of the Mejillones and Salar del Carmen faults. Along with the available geochronological, geochemical and paleoseismic data, our data supports the idea that co-seismic gypsum is formed during large earthquakes along major faults, and that this last phenomena could have occurred episodically at a rate in the order of 1:40 to 1:50 with respect to the very large subduction earthquakes during the latest Pleistocene and Holocene period. This superficial paleoseismic activity reflects deformation and reactivation of long-lived major faults, evidencing that these structures play a role in the absorption of inelastic deformation in the Andean subduction margin.

We conclude that an integrated approach involving U-series disequilibrium dating of gypsum salts, coupled with geomorphologic submarine and surface observations and radiocarbon dating can be used to refine the present model of earthquake recurrence in fault systems in the Atacama Desert and in other hyperarid and seismically active zones.

Acknowledgements

Support for this research was received from the International Earthquake Research Centre (CIIT-MB) grant P06-064-F, and FONDECYT grants 1070736 and 1085117. U–Th isotopic determinations were by the National Science Council grants 94-2116-M002-012, 97-2752-M002-004-PAE and -005-PAE. The authors thank Jacobus Le Roux for the revision of a previous version of this manuscript. Finally, we acknowledge Hans Thybo for handling the manuscript, Raul Madariaga and an anonymous reviewer for their insightful comments and suggestions.

References

Allmendinger, R.W., González, G., Yu, J., Hoke, G., Isacks, B., 2005. Trench-parallel shortening in the northern Chilean forearc: tectonic and climatic implications. Bulletin of the Geological Society of America 117, 89–104.

Angermann, D., Klotz, J., Reigber, C., 1999. Space-geodetic estimation of the Nazca-South America Euler vector. Earth and Planetary Science Letters 171, 329–334.

Arabasz, W.J., 1968. Geologic Structure of the Taltal area, northern Chile, in relation to the earthquake of December 28, 1966. Bulletin of the Seismological Society of America 58, 835–842.

Arabasz, W.J., 1971. Geological and Geophysical Studies of the Atacama Fault Zone in Northern Chile. Ph. D. Thesis, California Institute of Technology, Pasadena, 275 pp.

Armijo, R., Thiele, R., 1990. Active faulting in northern Chile—ramp stacking and lateral decoupling along a subduction plate boundary. Earth and Planetary Science Letters 98, 40–61.

Brodsky, E.E., Roeloffs, E., Woodcock, D., Gall, I., Manga, M., 2003. A mechanism for sustained groundwater pressure changes induced by distant earthquakes. Journal of Geophysical Research 108. doi:10.1029/2002JB002321.

Cameron, E.M., Leybourne, M.I., Kelley, D.L., 2002. Exploring for deeply-covered mineral deposits: formation of geochemical anomalies in northern Chile by earthquake-induced surface flooding of mineralized groundwaters. Geology 30, 1007–1010.

Cameron, E.M., Leybourne, M.I., Palacios, C., 2007. Atacamite in the oxide zone of copper deposits in northern Chile: involvement of deep formation waters? Mineralium Deposita 42, 205–218.

Cameron, E.M., Leybourne, M.I., Reich, M., Palacios, C., 2010. Geochemical anomalies in northern Chile as an expression of the extended supergene metallogenesis of buried copper deposits. Geochemistry: Environment, Exploration, Analysis 10, 1–14. doi:10.1144/1467-7873/09-228.

Caputo, R., Pavlides, S.B., 2008. Earthquake geology: methods and applications. Tectonophysics 453, 1–6.
Cheng, H., Edwards, R.L., Hoff, J., Gallup, C.D., Richards, D.A., Asmerom, Y., 2000. The half-lives of uranium-234 and thorium-230. Chemical Geology 169, 17–33.
Chlieh, M., Chabalier, J.B., Ruegg, J.C., Armijo, R., Dmowska, R., Campos, J., Feigl, K.L., 2004. Crustal deformation and fault slip during the seismic cycle in the North Chile subduction zone, from GPS and InSAR observations. Geophysics Journal of the Interior 158, 695–711.
Chung, L.-H., Chen, Y.-G., Wu, Y.-M., Shyu, J.B.H., Kuo, Y.-T., Lin, Y.-N.N., 2008. Seismogenic faults along the major suture of the plate boundary deduced by dislocation modeling of coseismic displacements of the 1951 M7.3 Hualien-Taitung earthquake sequence in eastern Taiwan. Earth and Planetary Science Letters 269, 416–426.
Colombani, J., 2008. Measurement of the pure dissolution rate constant of a mineral in water. Geochimica et Cosmochimica Acta 72, 5634–5640.
Comte, D., Pardo, M., 1991. Reappraisal of great historical earthquakes in the northern Chile and southern Peru seismic gap. Natural Hazards 4, 23–44.
Davisson, M.L., Presser, T.S., Criss, R.E., 1994. Geochemistry of tectonically expelled fluids from the northern Coast Ranges, Rumsey Hills, California, USA. Geochimica et Cosmochimica Acta 58, 1687–1699.
Delouis, B., Cisternas, A., Dorbath, L., Rivera, L., Kausel, E., 1996. The Andean subduction zone between 22 and 25°S (northern Chile): precise geometry and state of stress. Tectonophysics 259, 81–100.
Delouis, B., Monfret, T., Dorbath, L., Pardo, M., Rivera, L., Comte, D., Haessler, H., Caminade, J.P., Ponce, L., Kausel, E., Cisternas, A., 1997. The Mw = 8.0 Antofagasta (Northern Chile) earthquake of 30 July 1995; a precursor to the end of the large 1877 gap. Bulletin of the Seismological Society of America 87, 427–445.
Delouis, B., Philip, H., Dorbath, L., Cisternas, A., 1998. Recent crustal deformation in the Antofagasta region (northern Chile) and the subduction process. Geophysics Journal of the Interior 132, 302–338.
Delouis, B., Pardo, M., Legrand, D., Monfret, T., 2009. The Mw 7.7 Tocopilla earthquake of 14 November 2007 at the Southern Edge of the Northern Chile seismic gap: rupture in the deep part of the coupled plate interface. Bulletin of the Seismological Society of America 99, 87–94.
DeMets, C., Gordon, R.G., Argus, D.F., Stein, S., 1994. Effect of recent revisions to the geomagnetic reversal timescale on estimates of current plate motions. Geophysical Research Letters 21, 2191–2194.
Dorbath, L., Cisternas, A., Dorbath, C., 1990. Quantitative assessment of great earthquakes in Peru. Bulletin of the Seismological Society of America 80, 551–576.
Elkhoury, J.E., Brodsky, E.E., Agnew, D.C., 2006. Seismic waves increase permeability. Nature 441, 1135–1138.
González, G., Cembrano, J., Carrizo, D., Macci, A., Schneider, H., 2003. The link between forearc tectonics and Pliocene–Quaternary deformation of the Coastal Cordillera, northern Chile. Journal of South American Earth Science 16, 321–342.
González, G., Dunai, T., Carrizo, D., Allmendinger, R., 2006. Young displacements on the Atacama Fault System, northern Chile from field observations and cosmogenic ^{21}Ne concentrations. Tectonics 25. doi:10.1029/2005TC001846.
Gudmundsson, A., Simmenes, T.H., Larsen, B., Philipp, S.L., 2009. Effects of internal structure and local stresses on fracture propagation, deflection, and arrest in fault zones. Journal of Structural Geology. doi:10.1016/j.jsg.2009.08.013.
Houston, J., Hart, D., Houston, A., 2008. Neogene sedimentary deformation in the Chilean forearc and implications for Andean basin development, seismicity and uplift. Journal of the Geological Society 165, 291–306.
Kelleher, J.A., 1972. Rupture zones of large South American earthquakes and some predictions. Journal of Geophysics Research 77, 2087–2103.
Ku, T.L., 1976. The uranium-series methods of age determination. Annual Review of the Earth and Planetary Science 4, 347–379.
Ku, T.L., Luo, S., Lowenstein, T.K., Li, J., Spencer, R.J., 1998. U-series chronology of lacustrine deposits in Death Valley, California. Quaternary Research 50, 261–275.
Kurcer, A., Chatzipetros, A., Tuktum, S.Z., Pavlides, S., Ates, O., Valkaniotis, S., 2008. The Yenice-Gonen active fault (NW Turkey): active tectonics and paleoseismology. Tectonophysics 453, 263–275.
Lambeck, K., Esat, T., Potter, E.K., 2002. Links between climate and sea levels for the past three million years. Nature 419, 199–206.
Leybourne, M.I., Cameron, E.M., 2006. Composition of groundwaters associated with porphyry-Cu deposits, Atacama Desert, Chile: elemental and isotopic constraints on water sources and water–rock reactions. Geochimica et Cosmochimica Acta 70, 1616–1635.
Leybourne, M.I., Cameron, E.M., 2008. Source, transport, and fate of rhenium, selenium, molybdenum, arsenic, and copper in groundwater associated with porphyry-Cu deposits, Atacama Desert, Chile. Chemical Geology 247, 208–228.
Loveless, J.P., Pritchard, M.E., 2008. Motion on upper-plate faults during subduction zone earthquakes: case of the Atacama Fault System, northern Chile. Geochemical and Geophysical Geosystems 9. doi:10.1029/2008GC002155.
Loveless, J.P., Allmendinger, R.W., Pritchard, M.E., Garroway, J.L., Gonzalez, G., 2009. Surface cracks record long-term seismic segmentation of the Andean margin. Geology 37, 23–26.
Luo, S., Ku, T.-L., 1991. U-series isochron dating: a generalized method employing total sample dissolution. Geochimica et Cosmochimica Acta 55, 555–564.
MacFarlane, W.R., Kyser, T.K., Chipley, D., Beauchemin, D., Oates, C., 2005. Continuous leach inductively coupled plasma mass spectrometry; applications for exploration and environmental geochemistry. Geochemistry: Exploration, Environment, Analysis 5, 123–134.
Manga, M., Brodsky, E.E., Boone, M., 2003. Response of stream flow to multiple earthquakes. Geophysical Research Letters 30. doi:10.1029/2002GL016618.
Marquardt, C., 2005. Déformations Néogènes le long de la cotê nord du Chili (23°–27°S), avant-arc des Andes Centrales. Ph.D. Thesis, University of Toulouse-III, 212 pp.
Marquardt, C., Lavenu, A., Ortlieb, L., Godoy, E., Comte, D., 2004. Coastal neotectonics in Southern Central Andes: uplift rates and strain patterns in the Caldera Area, Northern Chile (27°S). Tectonophysics 394, 193–219.
Matsumoto, N., 1992. Regression-analysis for anomalous changes of ground-water level due to earthquakes. Geophysical Research Letters 19, 1193–1196.
Mogi, K., Mochizuki, H., Kurokawa, Y., 1989. Temperature changes in an artesian spring at Usami in the Izu peninsula (Japan) and their relation to earthquakes. Tectonophysics 179, 27–53.
Montgomery, D., Manga, M., 2003. Stream flow and water well responses to earthquakes. Science 300, 2047–2049.
Muir-Wood, R., 1994. Earthquakes, strain cycling and the mobilization of fluids. In: Parnell, J. (Ed.), Geofluids: Origin, Migration and Evolution of Fluids in Sedimentary Basins: Geological Society of London. Sp. Publ., 78, pp. 85–98.
Muir-Wood, R., King, G., 1993. Hydrological signatures of earthquake strain. Journal of Geophysical Research 98, 22,035–22,068.
Nishenko, S.P., 1985. Seismic potential for large and great interplate earthquakes along the Chilean and southern Peruvian margins of South America: a quantitative reappraisal. Journal of Geophysical Research 90, 3589–3615.
Nur, A., 1974. Matsushiro, Japan, earthquake swarm: confirmation of dilatancy-fluid diffusion model. Geology 2, 217–221.
Ohno, M., Sato, T., Notsu, K., Wakita, H., Ozawa, K., 2006. Groundwater level changes due to pressure gradient induced by nearby earthquakes off Izu peninsula, 1997. Pure and Applied Geophysics 163, 647–655.
Ortlieb, L., Zazo, C., Goy, J.L., Hillaire-Marcel, C., Ghaleb, B., Cournoyer, L., 1996. Coastal deformation and sea-level changes in the northern Chile subduction area (23°S) during the last 330 ky. Quaternary Science Reviews 15, 819–831.
Palacios, C., Guerra, N., Townley, B., Lahsen, A., Parada, M.A., 2005. Copper geochemistry in salts from evaporite soils, Coastal Range of the Atacama Desert, northern Chile: an exploration tool for blind Cu deposits. Geochemistry: Exploration, Environment, Analysis 5, 371–378.
Pritchard, M.E., Ji, C., Simons, M., 2006. Distribution of slip from 11 $Mw > 6$ earthquakes in the northern Chile subduction zone. Journal of Geophysical Research 111. doi:10.1029/2005JB004013.
Rech, J., Currie, B., Michalski, G., Cowan, A., 2006. Neogene climate change and uplift in the Atacama Desert, Chile. Geological Society of America 34 (9), 761–764. doi:10.1130/G22444.1.
Rech, J.A., Owen, L.A., Allmendinger, R.W., Baker, A., 2009. Assessing the Role of Seismic Pumping in the Formation of Co-seismic Soil Cracks, Atacama Desert, Chile. Portland Geological Society of America Annual Meeting. Paper No. 56-11.
Reich, M., Palacios, C., Parada, M.A., Fehn, U., Cameron, E.M., Leybourne, M.I., Zuñiga, A., 2008. Atacamite formation by deep saline waters in copper deposits from the Atacama Desert, Chile: evidence from fluid inclusions, groundwater geochemistry, TEM, and ^{36}Cl data. Mineralium Deposita 43, 663–675.
Reich, M., Palacios, C., Vargas, G., Luo, S., Cameron, E.M., Leybourne, M.I., Parada, M.A., Zuñiga, A., You, C.-F., 2009. Supergene enrichment of copper deposits since the onset of modern hyperaridity in the Atacama Desert, Chile. Mineralium Deposita 44, 497–504.
Roeloffs, E.A., 1998. Persistent water level changes in a well near Parkfield, California, due to local and distant earthquakes. Journal of Geophysical Research 103, 869–889.
Ruegg, J.C., Campos, J., Armijo, R., Barrientos, S., Briole, P., Thiele, R., Arancibia, M., Canuta, J., Duquesnoy, T., Chang, M., Lazo, D., Lyon-Caen, H., Ortlieb, L., Rossignol, J.C., Serrurier, L., 1996. The Mw = 8.1 Antofagasta earthquake of July 30, 1995: first results from teleseismic and geodetic data. Geophysical Research Letters 23, 917–920.
Scheuber, E., González, G., 1999. Tectonics of the Jurassic–early Cretaceous magmatic arc of the north Chilean Coastal Cordillera (22°–26°S): a story of crustal deformation along a convergent plate boundary. Tectonics 18, 895–910.
Shen, C.-C., Edwards, R.L., Cheng, H., Dorale, J.A., Thomas, R.B., Moran, S.B., Weinstien, S.E., Edmonds, H.N., 2002. Uranium and thorium isotopic and concentration measurements by magnetic sector inductively coupled plasma mass spectrometry. Chemical Geology 185, 165–178.
Shen, C.-C., Cheng, H., Edwards, R.L., Moran, S.B., Edmonds, H.N., Hoff, J.A., Thomas, R.B., 2003. Measurement of attogram quantities of ^{231} Pa in dissolved and particulate fractions of seawater by isotope dilution thermal ionization mass spectroscopy. Analytical Chemistry 75, 1075–1079.
Sibson, R.H., 1981. Fluid flow accompanying faulting: field evidence and models. In: Simpson, D.W., Richards, P.G. (Eds.), Earthquake Prediction: An International Review: American Geophysical Union, Maurice Ewing Series, 4, pp. 593–603.
Sibson, R.H., Moore, J.M., Rankin, A.H., 1975. Seismic pumping; a hydrothermal fluid transport mechanism. Journal of the Geological Society of London 131, 653–659.
Stuiver, M., Reimer, P.J., 1993. Extended ^{14}C database and revised CALIB radiocarbon calibration program. Radiocarbon 35, 215–230.
Taylor, M.H., Leprince, S., Avouac, J.P., Sieh, K., 2008. Detecting co-seismic displacements in glaciated regions: an example from the great November 2002 Denali earthquake using SPOT horizontal offsets. Earth and Planetary Science Letters 270, 209–220.
Uysal, T., Feng, Y., Zhao, J.-X., Altunel, E., Weatherley, D., Kurabacak, V., Cengiz, O., Golding, S.D., Lawrence, M.G., Collerson, K.D., 2007. U-series dating and geochemical tracing of late Quaternary travertine in co-seismic fissures. Earth and Planetary Science Letters 257, 450–462.
Vargas, G., Ortlieb, L., Chapron, E., Valdes, J., Marquardt, C., 2005. Paleoseismic inferences from a high-resolution marine sedimentary record in northern Chile (23°S). Tectonophysics 399, 381–398.

Vargas, G., Rutland, J., Ortlieb, L., 2006. ENSO tropical-extratropical climate teleconnections and mechanisms for Holocene debris flows along the hyperarid coast of western South America (17°–24°S). Earth and Planetary Science Letters 249, 467–483.

Vargas, G., Pantoja, S., Rutllant, J., Lange, C., Ortlieb, L., 2007. Enhancement of coastal upwelling and interdecadal ENSO-like variability in the Peru–Chile Current since late 19th century. Geophysical Research Letters 34. doi:10.1029/2006GL028812.

Wakita, H., 1975. Water wells as possible indicators of tectonic strain. Science 189, 553–555.

Wells, D., Coppersmith, K., 1994. New empirical relationships among magnitude, rupture length, rupture width, rupture area, a surface displacement. Bulletin of the Seismological Society of America 84, 974–1002.